T$_1$-weighted DCE Imaging Concepts: Modelling, Acquisition and Analysis

Paul S. Tofts, PhD

Brighton and Sussex Medical School, Falmer, Sussex, United Kingdom

1. Introduction

There are increasing opportunities to use Dynamic Contrast-Enhanced (DCE) T$_1$-weighted imaging to characterize tumor biology and treatment response, using the modern fast sequences that can provide good temporal and spatial resolution combined with good organ coverage [1]. Quantification in MRI is recognized as an important approach to characterize tissue biology. This article provides an introduction to the physics concepts of mathematical modelling, image acquisition and image analysis needed to measure aspects of tumor biology using DCE imaging, in a way that should be accessible for a research-minded clinician.

Quantification in MRI represents a paradigm shift, a new way of thinking about imaging [2]. In qualitative studies, the scanner is a highly sophisticated camera, collecting images that are viewed by an experienced radiologist. In quantitative studies, the scanner is used as a sophisticated measuring device, a scientific instrument able to measure many properties of each tissue voxel (e.g. T$_1$, T$_2$, diffusion tensor, magnetisation transfer, metabolite concentration, K^{trans}). An everyday example of quantification would be the bathroom scales, used to measure our weight. We expect that the machine output shown on the dial, in kg, will be accurate (i.e. close to the true value), reproducible (i.e. if we make repeated measurements over a short time they will not vary), reliable (the scales always work) and biologically relevant (the quantity of weight does indeed relate to our health). An example of a clinical measurement would be a blood test; we expect it to work reliably every time. This is the aspiration for quantitative MRI: that it should deliver a high quality measurement that relates only to the patient biology (and not the state of the scanner at the time of measurement).

The transfer constant K^{trans} (see below) characterizes the diffusive transport of low-molecular weight Gd chelates across the capillary endothelium [3]. It can be measured using DCE MRI, and has been widely used in imaging studies to characterize tumor biology and treatment response. The fractional volume v$_e$ of the extravascular extracellular space (EES; i.e. the interstitial space), can also be measured. A consensus recommendation [4] proposed that in assessing anti-angiogenic and anti-vascular therapies, K^{trans} should be a primary endpoint. Secondary endpoints should include v$_e$, the rate constant k$_{ep}$ (k$_{ep}$=K^{trans}/v$_e$) and the plasma volume v$_p$ (if available). The traditional clinical evaluation of tumor treatment is the RECIST criterion, based on tumor diameter; however a tumor could die but not shrink, and K^{trans} and v$_e$ may often be more sensitive markers of tumor metabolism. There are also applications of DCE-MRI in tissues other than tumors, e.g. renal and myocardial function; this article focuses on tumor applications, with one example of renal function.

2. MRI modelling

Before any pharmacokinetic analysis can take place, the Gd contrast agent (CA) concentration has to be found from the MRI signal enhancement. This requires an MRI model, which has two components. First, T$_1$ is reduced by the presence of CA (eqn. 1 see appendix). The relaxivity r$_1$, (i.e. the constant of proportionality between Gd concentration and increase in relaxation rate R$_1$=1/T$_1$) is usually assumed to be equal to the in-vitro value (measured in aqueous phantoms), although it can alter in-vivo. The native T$_1$ of the tumor (i.e. the value before injection of CA, T$_{10}$) must also be known. Second, the way in which the T$_1$ reduction increases the signal is modelled (eqn. 3); this is specific to each sequence type, and also requires accurate knowledge of the flip angle FA. The most common sequence is the simple gradient echo (FLASH), on account of its speed; the sequence must be truly spoilt (i.e. there is no build up of steady state transverse magnetisation). Provided

these 3 parameters (r$_1$, T$_{10}$, FA) are known then there is a clear relationship between signal and Gd concentration.
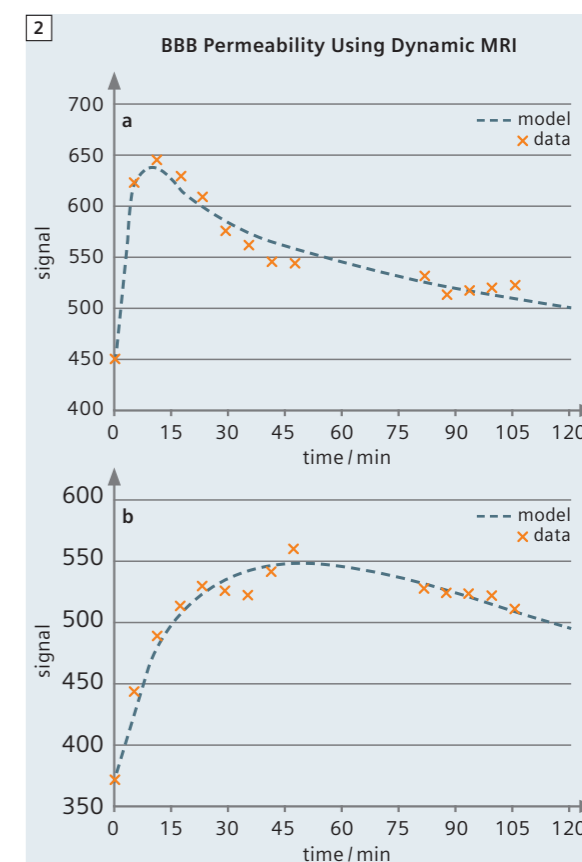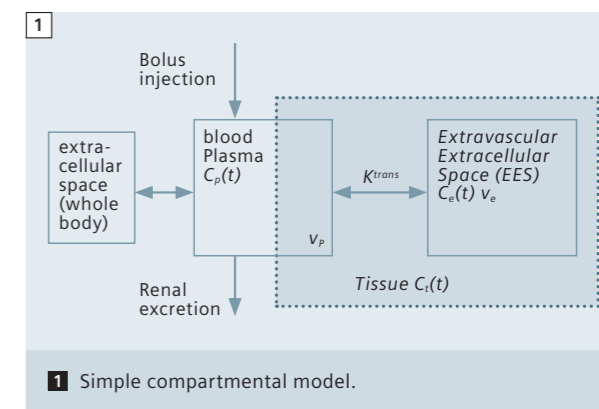
Some studies attempt to find Gd concentration from signal by using a phantom calibration curve; however these approaches are usually flawed, since the signal is also proportional to proton density (which is greater in an aqueous solution than in tissue), and the FA may be different when imaging the phantom (caused for example by different coil loading or B$_1$ inhomogeneity). The plasma concentration (required for the pharmacokinetic modelling – see below) may be measured from the blood signal. In this case, blood concentration is first found from the blood signal (using eqn. 3). The plasma concentration is about 70% higher, once haematocrit is taken account of (eqn. 4).
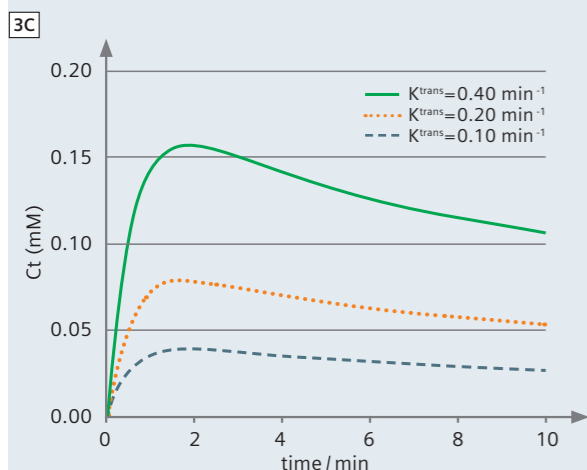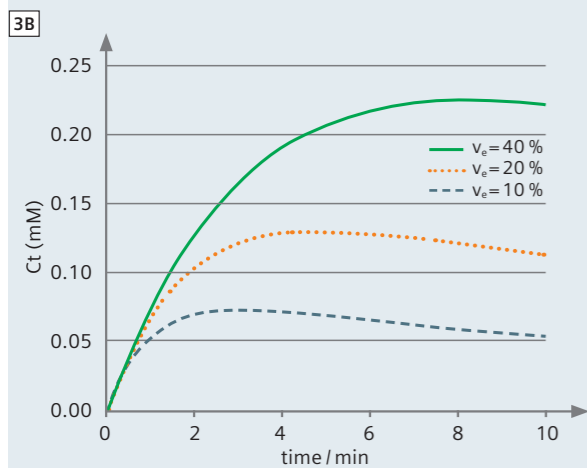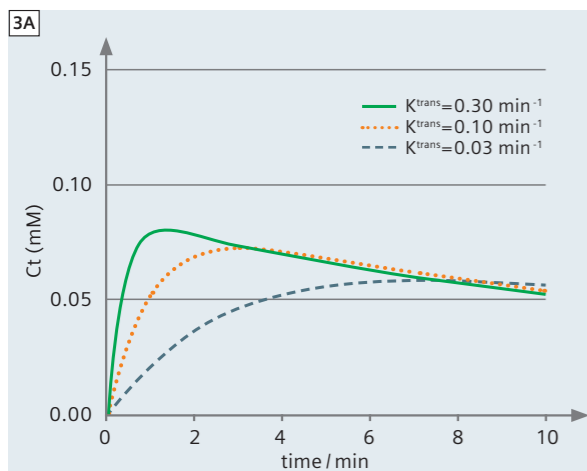
3. Pharmacokinetic modelling

Given the Gd concentration as a function of time, pharmacokinetic analysis can now be undertaken to model how the CA distributes in the body, and how this depends on characteristics of the tumor biology This is independent of the imaging conditions (MRI field strength etc.), and in principle even independent of imaging modality (CT or MRI). Most modelling uses the concept of a compartment; this is like a bucket: the Gd tracer inside is dissolved in water and at the same concentration everywhere, and the flow into or out of the bucket is small enough to allow the contents to remain well mixed.

The simplest compartmental model has one tissue compartment in addition to a vascular compartment; the so called 'Tofts model' [5] (mathematically equivalent to that proposed by Kety [6] in a non-MRI context), used to measure K^{trans} and v$_e$ (see fig. 1). The bolus injection of Gd gives a time-varying blood plasma concentration C$_p$(t), which can be measured in each subject, or else a population average can be used. Since the commonly used contrast agents are small (<≈ 1000 Daltons) then the leakage from the capillaries into the EES is diffusive and hence reversible; it is therefore proportional to the difference in concentrations, and K^{trans} is the constant of proportionality (eqn. 5).

The total Gd concentration in a voxel or ROI (eq 6) is the sum of the EES contribution (which usually dominates, since v$_e$ ≈ 10–60%) and the intravascular contribution (the 'vp term') which is often small and ignored (v$_p$ ≈ 1–10%) [7].

This model was able to explain signal enhancement in multiple sclerosis lesions [5] (fig. 2), and gave values of K^{trans} and v$_e$ consistent with the known biology of acute and chronic lesions.

1 Simple compartmental model.

2 First case of DCE-MRI to measure capillary leakage, published in 1991 by Tofts and Kermode [5]. The upper plot shows enhancement in an acute multiple sclerosis lesion. The signal peaks at about 12 min, model fitting gave K^{trans} = 0.050 min^{-1}, v$_e$ = 21%. The lower plot shows a chronic lesion with a less permeable blood-brain barrier (K^{trans} = 0.013 min^{-1}), and an enlarged EES (v$_e$=49%), with signal peaking later (at about 50 min). These data were collected in 1989 using a multislice spin echo sequence; note the poor temporal resolution by modern standards, and the missing data when the patients took a break. *(Reproduced from Magn Reson Med 1991).*

3A

3B

3 Simulations of tissue concentration after bolus injection of 0.1 mmole/kg of Gd, for a range of K^{trans} and v_e values, ignoring any IV contribution.
(A) Increasing K^{trans}, with fixed v_e = 10%.
(B) Increasing v_e, with fixed K^{trans} = 0.1 min^{-1}.
(C) Constant k_{ep} = 2 min^{-1}, increasing K^{trans}.

The differences in enhancement curve shape, and the time of peak enhancement, both apparent in fig. 2, are important. A model simulation [5] using typical K^{trans} values for tumors shows that the initial slope depends on K^{trans} (fig. 3A), and is independent of v_e (fig. 3B). The final peak value depends on v_e, and larger v_e tumors take longer to reach their peak (fig. 3B). The shape of the curve is determined by k_{ep}, and if K^{trans} is increased whilst keeping k_{ep} fixed, the curve increases in amplitude but retains the same shape (fig. 3C) as is expected from equation 6.

In the original formulation of the model (applied to multiple sclerosis), trans-endothelial leakage was low enough that there would not be significant local depletion of Gd concentration in the capillary. Perfusion F was sufficient to maintain the capillary concentration at the arterial value. In this case, K^{trans} is just the permeability surface area product (PS), and DCE could reasonably be called permeability imaging'. This 'permeability-limited' case is defined by F≪PS. In tumors, the endothelium can be much more leaky, there may be local depletion, and K^{trans} will represent a combination of permeability and perfusion [3]. In the limiting case of very high permeability, then K^{trans} will equal perfusion, and DCE could reasonably be called 'perfusion imaging'. This is the 'flow-limited case', defined by F≪PS.

The modelling of the capillary vasculature shown in figure 1 is naive, and not surprisingly at high temporal resolution it fails. Modern sequences can sometimes provide a temporal resolution of ~1 s (depending on the organ and the coverage required), and in these cases the initial rise in signal gives information about perfusion, as Gd arrives in the capillary bed over a few seconds. More sophisticated models are then able to extract pure perfusion information [8, 9], and potentially pure permeability information as well. In DCE kidney imaging, the perfusion peak in tissue is clearly delayed (by about 4 s) with respect to the arterial peak (see fig. 5).

4. Image acquisition

In DCE imaging, repeated T_1-weighted images are collected for several frames before Gd is injected, and then for several minutes afterwards. This is often preceded by a T_1 measurement. A good bolus injection can be achieved by using a power injector, with a saline flush after the Gd. The receiver gain must be controlled for the whole series of DCE images.
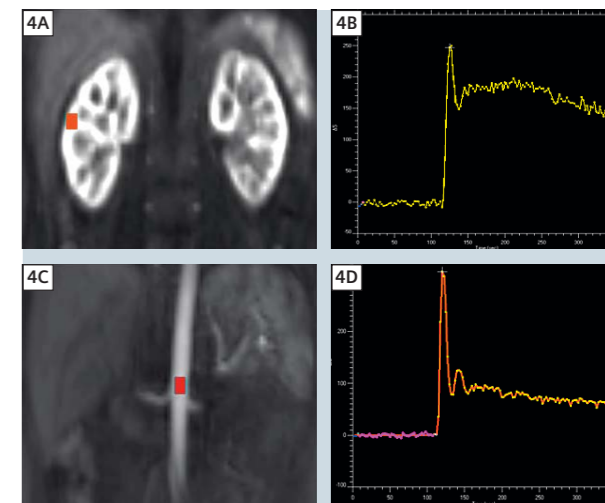
Quality assurance [2] can be used to ensure the scanner is stable for the DCE acquisition period. Either a phantom can be repeatedly imaged (this can also be used to check T_1 accuracy), or a volunteer can be repeatedly scanned (without Gd).

The sequence parameters will involve compromise between coverage, temporal resolution and spatial resolution. Newer scanners have faster gradients (allowing shorter TR's), and multi-array receive coils give higher SNR at short TR's. The optimal sequence will depend on the organ being measured; often frame times of 2–20 s can be achieved. 3D (volume) sequences are preferred, since they have better FA accuracy than 2D (slice selective) sequences. Body coil transmission gives better FA accuracy than combined transmit/receive coils. In the abdomen, a coronal-sagittal oblique slice orientation (instead of transverse) has two advantages: the aorta can be sampled along its length, removing wash-in effects, and breathing movement is mostly in-plane and therefore more easily corrected.
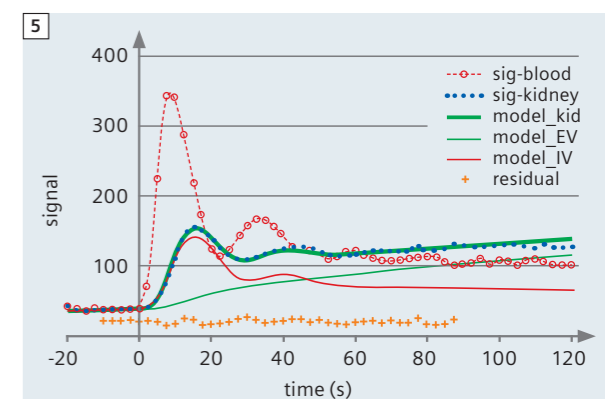
The blood curve may be measured, in order to provide an AIF for the modelling. In this case a temporal resolution of ~3 s or less is desirable, and it is usually the aorta that is imaged. Wash-in effects are reduced by ensuring that the blood is fully saturated (i.e. has experienced several RF pulses) by the time it reaches the location of the region of interest (ROI).

The DCE sequence should ideally be run long enough to sample the enhancement plateau. If not, then v_e cannot be reliably measured, since it does not affect the rising part of the curve, only the plateau value (see fig. 3B). An example of rapid DCE is shown in figure 4. Imaging of the kidney and aorta at a temporal resolution of 2.5 s, using half standard dose of Gd, allows the perfusion phase of the tissue signal to be seen, and it has a clear delay with respect to the aortic peak. In this organ the blood volume is large (about 30%), and can be estimated because the perfusion peak is so distinct. A modified model fits the data well (fig. 5); in this model of the uptake phase (up to 90 s), the vascular delay and dispersion are accounted for, and there is no efflux from the parenchymal ROI. Renal filtration occurs mostly after bolus passage, and can be well estimated. GFR estimates in controls are in good agreement with normal values (reference 10 and manuscript in preparation).

There is scope to optimise the FA. A small FA gives more signal at low concentration, but has limited dynamic range (see fig. 6 FA = 5°); increasing the FA gives increased sensitivity to Gd (fig. 6 FA = 10°); further increases (fig. 6 FA = 20° or 30°) give a wider dynamic range (at the expense of reduced sensitivity) and are needed if measuring the AIF (peak blood concentration 6mM [11] and see fig. 7 below) as well as tissue enhancement. Nonlinearity is not a concern as it is properly dealt with in the MRI model.
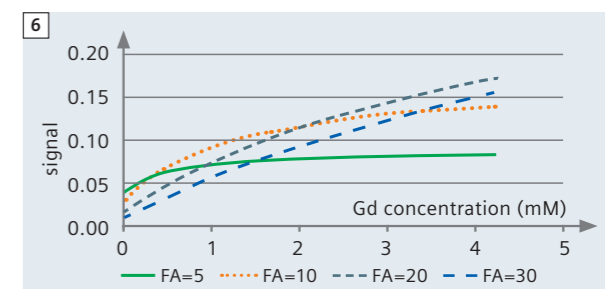
Breathing causes serious artifacts in body imaging. There are several approaches to minimising its effect:

4 Signal enhancement in kidney and aorta. A cortical ROI **(A)** is used to define the time of peak enhancement **(B)** and hence the arterial ROI **(C)** giving the blood curve **(D)**.

5 Model analysis of renal enhancement. The kidney signal (sig-kidney) is clearly delayed (by about 2 time points) from the blood signal (sig-blood). The model fit (model-kid) shows separately the extravascular filtered Gd (model-EV, from which GFR is found) and the intravascular Gd (model-IV, from which blood volume and perfusion are estimated).

6 Performance of gradient echo sequence with various FA values. Eqns 2 and 3 were used, with TR = 3 ms; T_1 = 1 s.

i) Allow free breathing and minimise diaphragm movement by having hands above the head. This can be uncomfortable; having a single hand above the head is easier and nearly as effective.

ii) Breath-hold for first pass (~20 s) then allow breathing (although this can result in a large movement as breathing resumes).

iii) Free breathe and discard data at the extremes of position (using the images or respiratory monitoring to detect the extrema).

iii) Guided free breathing (instructions from the imaging radiographer).

Whether breathing should be controlled or not is currently unclear (this may depend on the kind of patient, and the availability of registration – see below), and is the subject of ongoing research.

Flip angle accuracy is often poor yet crucial in determining the accuracy of the K^{trans} value. It affects the calculation of concentration from enhancement (eq. 3), the estimation of the AIF, and the measurement of T_{10}. B_1 nonuniformity (heterogeneity), if present, means that the FA distribution is also nonuniform. There are two primary causes of such nonuniformity. Firstly, dielectric resonance produces standing waves in the subject, which are more pronounced at higher fields (≥3T), and in larger objects (the effect is greater in the body than in the head). Secondly, smaller transmit coils are less uniform, and therefore the body transmit coil is to be preferred (not a smaller combined transmit/receive coil). During the FA setup procedure, a good technique will optimise the FA over just the volume to be imaged (not the whole slice), and an accurate FA may then be obtained in spite of more global FA nonuniformity. An additional source of FA error is in 2D multislice imaging, where the slice profile is often poor, and a

distribution of FA values exists across the slice. Therefore 3D (volume) acquisitions are preferred. B_1 maps can be measured quite quickly [12] (<2 min) and these may enable corrections to be made in the presence of FA inaccuracy and inhomogeneity. Phased transmit array technology is in development (essential for imaging >3T). This gives impressive control over B_1 at each location in the subject, and such 'RF shimming' is expected to give uniform and accurate FA values. The tissue T_1 value (T_{10}) can be measured, or else a standard value from the literature used. An accurate measurement is preferred for each individual subject, since in disease this can alter; this can often be carried out in < 5 minutes. The most common method is the variable flip angle method, where gradient echo sequences with several FA values are used. These include a mostly PD-weighted sequence (low FA) and one or more T_1-weighted sequence (higher FA). Clearly the T_{10} accuracy is crucially dependent on the FA accuracy. Inversion recovery methods (with variable TI, fixed FA) are more robust, but usually slower. The measured K^{trans} value is very sensitive to the accuracy of the T_{10} value. An example from breast cancer shows that [13] for a range of feasible T_{10} values, the fits are equally good, K^{trans} can vary by at least a factor of 2, and v_e can reach impossible values (v_e>100%); see table 1. k_{ep} is relatively robust. An increase of 1% in T_{10} gives a resulting decrease of 1% in K^{trans}, such that the product remains approximately constant.

Any low molecular weight contrast agent can in principle be used for DCE methodology. The initial work [5] was carried out with Gd-DTPA, size 570D, and then with Magnevist (938D). Clearly larger molecules will have lower permeability and hence K^{trans} values, and the AIF may alter a little with viscosity. In view of the con-

cerns about NSF, there will be value in gaining experience using the newer cyclic compounds. Potentially suitable candidate compounds are as follows. Dotarem (754D), Eovist (725D), Gadovist (605D), Magnevist (938D), Multihance (1058D), Omniscan (574D), Optimark (662D), Primovist (685D), Prohance (559D) and Teslascan (757D) (see http://www.rxlist.com).
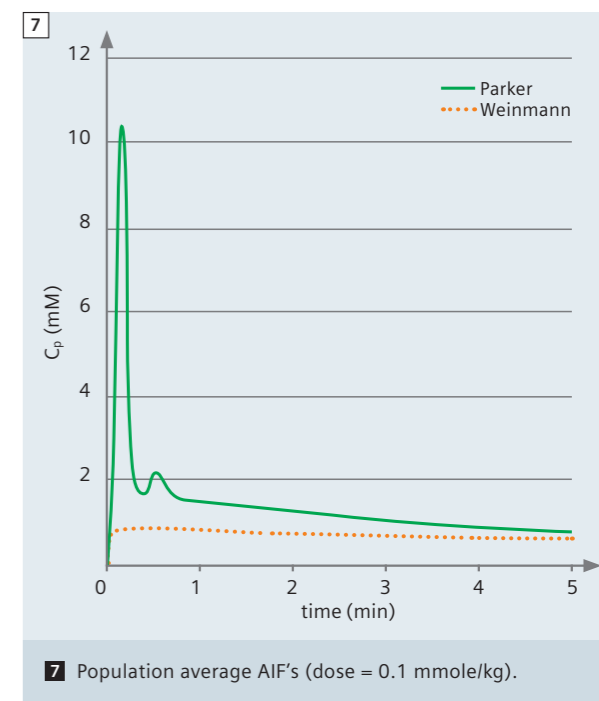
5. Image analysis

Analysis can be carried out on individual ROI's, or on a pixel-by-pixel basis to produce a map for the whole organ. The reduction of motion artefact using spatial registration, if available, is likely to improve the quality of the fit (depending on the tissue location). Because the motion is non-rigid, effective removal is much harder than in the brain, and a topic of ongoing research. In-plane movement is relatively easy to reduce. The pharmacokinetic model requires knowledge of the arterial plasma concentration $C_p(t)$; this arterial input function (AIF) can be calculated from the blood signal (which confusingly can also be called the AIF!). It can be measured for each subject, and thus within- and between-subject variation can be taken into account, although if the technique is not implemented well it can introduce extra variation which contaminates the final measurements of tissue physiology. Alternatively a population average AIF can be used. Some of these are described analytically (i.e. using mathematical equations, rather than just a list of numbers), which makes them more convenient to use. In particular they are available at any temporal resolution. The most popular are the original biexponential Weinmann plasma curve [5], derived from low temporal resolution arterial blood samples, and the more complex Parker blood function [11], derived from high temporal resolution MRI data. In the Parker function, bolus first pass and recirculation are represented. After bolus passage and recirculation, the MRI measurement (Parker C_p(1 min) = 1.53 mM assuming Hct = 42%) is 86% higher than the direct measurement (Weinmann C_p(1 min) = 0.82 mM). The possible reasons for this discrepancy include a population difference and wash-in effects in the MRI method. The numerical AIF's of Fritz-Hansen [14] showed excellent agreement between an inversion recovery MRI method and direct blood measurements; their values (average over 6 subjects C_p(1 min) = 1.09 mM) are closer to the Weinmann value. The choice of AIF will depend on the tissue being studied and the sequences available.

When it comes to the modelling, several versions can be considered. The primary free parameters are K^{trans} and either k_{ep} or v_e (since k_{ep} and v_e are related). It is
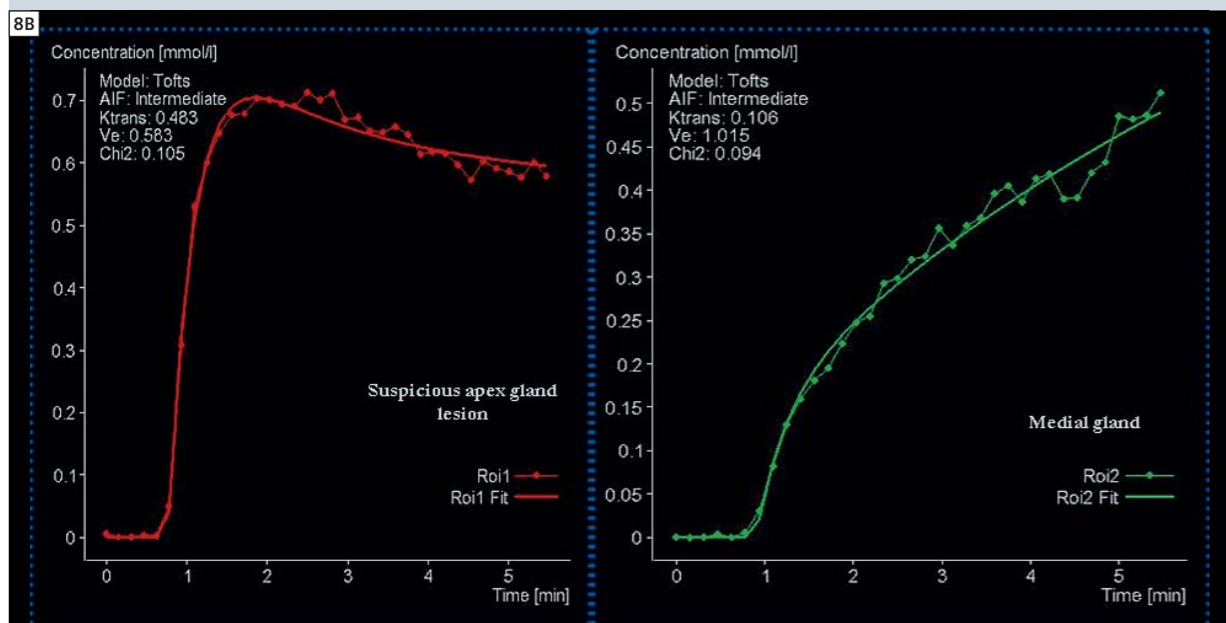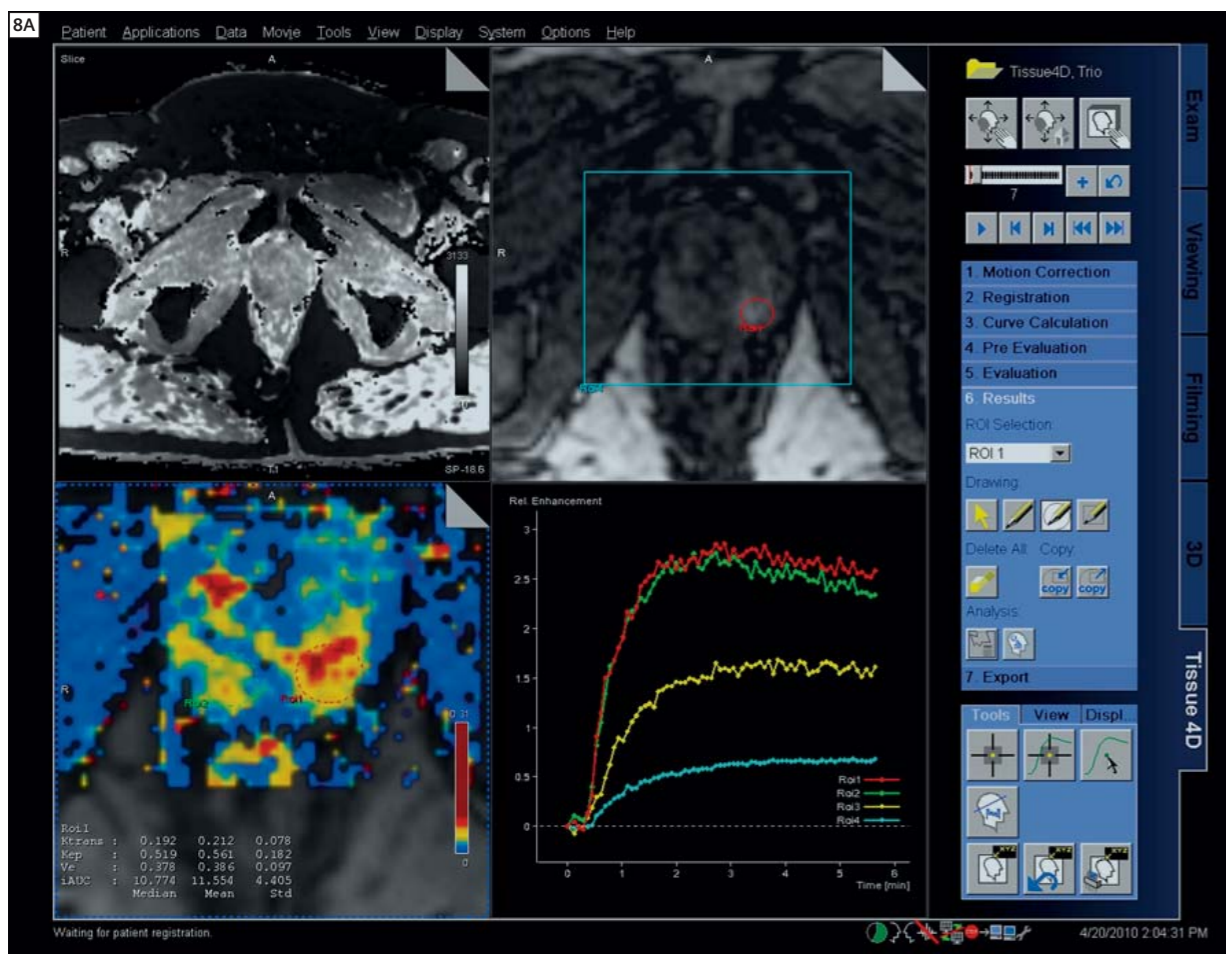

7 Population average AIF's (dose = 0.1 mmole/kg).

worth including v_p to see if the fit improves. The onset time of the bolus t_onset will be needed if a population average AIF is used (since the timing of bolus arrival with respect to the start of tissue enhancement is unknown). The appropriate approach will again depend on the organ and the temporal resolution.

The mathematical process of fitting the model to the data works as follows. The model signal can be calculated for many combinations of the free parameters (K^{trans} etc. see table 2 below). For each of these combinations, the differences between the model signal value (at each time point) and the measured data are found. These differences are squared and summed across each time point to provide a 'total difference'. The free parameters are adjusted until this total difference is minimised. The model has then been 'fitted' to the data. This is called the 'least squares solution'. The differences between the data and the fitted model are called 'residuals' (see e.g. fig. 5). From these can be found the 'root-mean-square residual', which is a kind of average difference between the model and the data, and which gives an indication of the quality of the model and of the fit. If the residuals appear random in character then these probably derive from a random effect such as image noise or movement; if there seems to be a systematic pattern to the residuals then the model can often be improved.

'Fit failures' can occur, particularly if the data are noisy (e.g. deriving from single pixels instead of a ROI); no

Table 1: Sensitivity of tissue parameters to T_{10} value. *(Adapted from Tofts 1995 [13])*

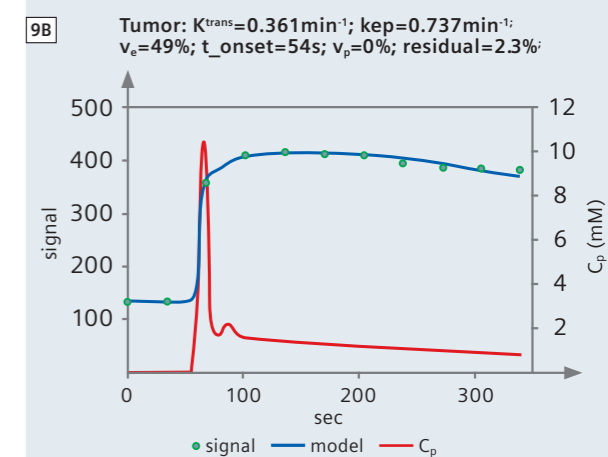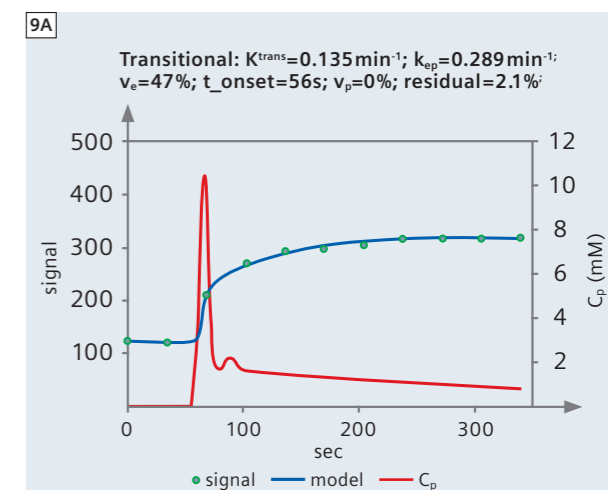| Tissue	T_{10} (s)	K^{trans} (min^{-1})	v_e (%)	residual in fit	k_{ep} (min^{-1})	$K^{trans} T_{10}$
Normal low risk fatty portion	0.46	0.88	143	0.091	0.62	0.41
Tumor – low T_1	0.60	0.63	96	0.092	0.65	0.38
Normal high risk diffuse density portion	0.71	0.51	76	0.093	0.67	0.36
Tumor – high T_1	1.3	0.26	36	0.095	0.72	0.34

8 **(A)** Tissue4D output. The workflow includes motion correction and registration. **(B)** Fit to data from prostate ROI's.

valid parameter values are produced for that dataset. In the fitting process it is important to identify and flag these failures, so that the output (i.e. invalid parameter values) does not contaminate any subsequent analysis. Values of $v_e > 100\%$ may occur if an incorrect value of T_{10} has been used (see table 1), or if the enhancement peak has not been reached (see fig. 3B).

Fitting can be implemented in two ways. The simplest way is to use ROI data (which are inherently low noise) and put these into a spreadsheet (e.g. Microsoft Excel running on a PC). The mathematics can be set up using inbuilt formula functions, and the 'solver' function can carry out the minimisation process. This does of course require some mathematical and computer ability. The more complex way is to set up pixel-by-pixel mapping, either using a standard environment (e.g. matlab) or by obtaining this from a supplier. Pixel mapping almost certainly needs spatial registration of the images to reduce the effect of motion; the operation is much more computer-intensive, and the single-pixel data are inherently noisy, so care must be taken to identify fit failures. The benefits of pixel mapping include the abilities to interrogate all the tissue without bias, and to generate histograms.

Histograms can show the distribution of parameter values, in a Region- or Volume-of-Interest. By taking care of histogram generation and architecture, histograms become more useful and comparisons are more easily made [15]. The y-values can be calculated such that the area under the histogram curve is either the total volume under interrogation (in mL), or 100%. By taking account of bin width, the histogram amplitude becomes virtually independent of bin width, and in a multicenter brain MTR study the intercenter difference was completely eliminated [16]. Features such as peak location and height can be extracted from histograms. Characterising the distribution tails can have predictive value [17, 18], and principle component analysis of the histogram shape can be powerful [19].

An example of a quite comprehensive software package to carry out pixel-by-pixel analysis is Tissue4D (fig. 8). The various functions needed are provided in a single workflow scheme, and ROI analysis is also available (this is useful to evaluate the quality of the modelling). An example of using a spreadsheet to implement modelling of ROI data is shown in figure 9. The prostate data have quite low temporal resolution (34 s), T_{10} had to be assumed (1.5 s), and a Parker AIF was used. Including the v_p term did not improve the fitting (and in fact it became rather unstable). In several ROI's from the same subject, fitted onset time agreed within 2 s, suggesting that it can be found quite reliably.

Transitional: $K^{trans}=0.135\,min^{-1}$; $k_{ep}=0.289\,min^{-1}$; $v_e=47\%$; t_onset=56s; $v_p=0\%$; residual=2.1%;

Tumor: $K^{trans}=0.361\,min^{-1}$; kep=0.737min^{-1}; $v_e=49\%$; t_onset=54s; $v_p=0\%$; residual=2.3%;

9 Modelling of prostate cancer DCE data. The Parker AIF was used (fig. 7), with $v_p=0$. Although data were only acquired every 34 s, the model was calculated with a temporal resolution of 1 s. Spreadsheet output is shown for transitional tissue **(A)** and tumor **(B)** ROI's. *(Data from University of Miami.)*

6. Conclusions

The principle physiological parameters that can be measured with DCE-MRI are the transfer coefficient K^{trans} (related to capillary permeability, surface area and perfusion) and v_e the size extravascular extracellular space. To do this needs good control of flip angle and an accurate measurement of tissue T_1 before injection of Gd. If T_1 is not available, then it may be possible to use a standard value; in any case the rate constant k_{ep} can still be measured, which is probably useful. The possible and optimum acquisition protocols and models will depend on which tissue is being imaged. Spread sheet analysis can provide quick access to modelling.

Acknowledgements

Appendix

MRI model

T_1 is reduced from its native value T_{10} by the presence of a concentration C of Gd:

$$\frac{1}{T_1} = \frac{1}{T_{10}} + r_1 C$$

Equation 1

r_1 is the relaxivity, and usually an in-vitro value of 4.5 s^{-1} mM^{-1} is used. Often it is more convenient to use the relaxation rate:

$$R_1 = R_{10} + r_1 C$$

Equation 2

Note that to apply eqns 1 and 2 to total tissue Gd concentration implicitly assumes fast exchange i.e. that all the Gd in a voxel is available to relax all of the water. The signal S from a spoilt gradient echo sequence (i.e. FLASH) is:

$$S = S_0 \frac{(1 - e^{-TR/T_1})\sin\theta}{1 - e^{-TR/T_1}\cos\theta}$$

Equation 3

where S_0 is the relaxed signal (TR≫T_1, θ=90°), and θ is the FA. S_0 can be found from the measured pre-Gd signal (before injection of CA).

To find the plasma concentration (if required), firstly the blood concentration $C_b(t)$ is found from the blood signal, using eqns 1 and 3. Blood T_{10} is about 1.4 s [20]. The plasma concentration $C_p(t)$ is higher, by a factor related to the haematocrit Hct (typically 42%):

$$C_p = \frac{C_b}{1 - Hct}$$

Equation 4

Pharmacokinetic model

The flow of Gd across the endothelium into the EES is

$$v_e \frac{dC_e(t)}{dt} = K^{trans}(C_p(t) - C_e(t))$$

Equation 5

The solution to this is [7] a convolution of C_p with the impulse response function $K^{trans} \exp(-k_{ep}t)$; when the IV Gd is taken into account, the total tissue concentration is:

$$C_t(t) = v_p\, C_p(t) + K^{trans} \int_0^t C_p(\tau) e^{-k_{ep}(t-\tau)} d\tau$$

Equation 6

Model parameters

There are several kinds of parameters used in the model. *Fixed* parameters (*FA TR Hct T_{10} T_{10}^{blood} r_1*) have preset values which are required before fitting can start. *Free* parameters (K^{trans} v_e k_{ep} and maybe v_p and t_onset) are varied and then estimated as part of the fitting process. Other parameters (C_p etc) are used temporarily as part of the process of modelling the signal. The fixed and free parameters are summarised in table 2.

Table 2: Fixed and free parameters in DCE modelling.

Quantity	symbol	units	type
flip angle[a]	FA	degrees	fixed
haematocrit	Hct	%	fixed (42%)
onset time	t_onset	s	free
rate constant[b]	k_{ep}	min^{-1}	free
transfer constant	K^{trans}	min^{-1}	free
T_1 relaxivity	r_1	s^{-1} mM^{-1}	fixed (4.5 s^{-1} mM^{-1})
T_1 of blood	T_{10}^{blood}	s	fixed (1.4 s)
T_1 of tissue	T_{10}	s	fixed
TR	TR	s	fixed
fractional volume of EES[c]	v_e	0<v_e<100%	free
fractional volume of blood plasma in tissue	v_p	0<v_p<100%	free

[a] θ is the flip angle in radians, [b] $k_{ep} = K^{trans}/v_e$, [c] Extravascular Extracellular Space

References

1 Jackson A, Buckley DL, Parker GJ. Dynamic Contrast-Enhanced Magnetic Resonance Imaging in Oncology. Springer, 2004.
2 Tofts PS. Quantitative MRI of the brain: measuring changes caused by disease. John Wiley, 2003.
3 Tofts PS, Brix G, Buckley DL, Evelhoch JL, Henderson E, Knopp MV, Larsson HB, Lee TY, Mayr NA, Parker GJ, Port RE, Taylor J, Weisskoff RM. Estimating kinetic parameters from dynamic contrast-enhanced T(1)-weighted MRI of a diffusable tracer: standardized quantities and symbols. J Magn Reson Imaging 1999;10:223-232.

4 Leach MO, Brindle KM, Evelhoch JL, Griffiths JR, Horsman MR, Jackson A, Jayson GC, Judson IR, Knopp MV, Maxwell RJ, McIntyre D, Padhani AR, Price P, Rathbone R, Rustin GJ, Tofts PS, Tozer GM, Vennart W, Waterton JC, Williams SR, Workman P. The assessment of antiangiogenic and antivascular therapies in early-stage clinical trials using magnetic resonance imaging: issues and recommendations. Br J Cancer 2005;92:1599-1610.
5 Tofts PS, Kermode AG. Measurement of the blood-brain barrier permeability and leakage space using dynamic MR imaging. 1. Fundamental concepts. Magn Reson Med 1991;17:357-367.

6 Kety SS. The theory and applications of the exchange of inert gas at the lungs and tissues. Pharmacol Rev 1951;3:1-41.
7 Tofts PS. Modeling tracer kinetics in dynamic Gd-DTPA MR imaging. J Magn Reson Imaging 1997;7:91-101.
8 St Lawrence KS, Lee TY. An adiabatic approximation to the tissue homogeneity model for water exchange in the brain: I. Theoretical derivation. J Cereb Blood Flow Metab 1998;18:1365-1377.
9 Donaldson SB, West CM, Davidson SE, Carrington BM, Hutchison G, Jones AP, Sourbron SP, Buckley DL. A comparison of tracer kinetic models for T1-weighted dynamic contrast-enhanced MRI: application in carcinoma of the cervix. Magn Reson Med 2010;63:691-700.
10 Tofts PS, Cutajar M, Mendichovszky IA, Gordon I. Accurate and precise measurement of renal filtration and vascular parameters using DCE-MRI and a 3-compartment model. Proc Intl Soc Mag Reson Med, 18th annual meeting, Stockholm.2010; 326.
11 Parker GJ, Roberts C, Macdonald A, Buonaccorsi GA, Cheung S, Buckley DL, Jackson A, Watson Y, Davies K, Jayson GC. Experimentally-derived functional form for a population-averaged high-temporal-resolution arterial input function for dynamic contrast-enhanced MRI. Magn Reson Med 2006;56:993-1000.
12 Dowell NG, Tofts PS. Fast, accurate, and precise mapping of the RF field in vivo using the 180 degrees signal null. Magn Reson Med 2007;58:622-630.
13 Tofts PS, Berkowitz B, Schnall MD. Quantitative analysis of dynamic Gd-DTPA enhancement in breast tumors using a permeability model. Magn Reson Med 1995;33:564-568.
14 Fritz-Hansen T, Rostrup E, Larsson HB, Sondergaard L, Ring P, Henriksen O. Measurement of the arterial concentration of Gd-DTPA using MRI: a step toward quantitative perfusion imaging. Magn Reson Med 1996;36:225-231.
15 Tofts PS, Davies GR, Dehmeshki J. Histograms: measuring subtle diffuse change (chapter 18). In: Paul Tofts, editor. Quantitative MRI of the brain: measuring changes caused by disease. Chichester: John Wiley, 2003: 581-610.

16 Tofts PS, Steens SC, Cercignani M, Admiraal-Behloul F, Hofman PA, van Osch MJ, Teeuwisse WM, Tozer DJ, van Waesberghe JH, Yeung R, Barker GJ, van Buchem MA. Sources of variation in multi-centre brain MTR histogram studies: body-coil transmission eliminates inter-centre differences. Magn Reson Mater Phy 2006;19:209-222.
17 Tofts PS, Benton CE, Weil RS, Tozer DJ, Altmann DR, Jager HR, Waldman AD, Rees JH. Quantitative analysis of whole-tumor Gd enhancement histograms predicts malignant transformation in low-grade gliomas. J Magn Reson Imaging 2007;25:208-214.
18 Donaldson SB, Buckley DL, O'Connor JP, Davidson SE, Carrington BM, Jones AP, West CM. Enhancing fraction measured using dynamic contrast-enhanced MRI predicts disease-free survival in patients with carcinoma of the cervix. Br J Cancer 2010;102:23-26.
19 Dehmeshki J, Ruto AC, Arridge S, Silver NC, Miller DH, Tofts PS. Analysis of MTR histograms in multiple sclerosis using principal components and multiple discriminant analysis. Magn Reson Med 2001;46:600-609.
20 Spees WM, Yablonskiy DA, Oswood MC, Ackerman JJ. Water proton MR properties of human blood at 1.5 Tesla: magnetic susceptibility, T(1), T(2), T*(2), and non-Lorentzian signal behavior. Magn Reson Med 2001;45:533-542.